LASER INTERFEROMETER GRAVITATIONAL WAVE OBSERVATORY
- LIGO -
CALIFORNIA INSTITUTE OF TECHNOLOGY
MASSACHUSETTS INSTITUTE OF TECHNOLOGY

Technical Note	**LIGO-T2300208–vX**	2023/09/20

Frequency Stabilization of 2 Micron Lasers Using Optical Delay Self-Heterodyne Interferometry

Stella Kraus

California Institute of Technology
LIGO Project, MS 18-34
Pasadena, CA 91125
Phone (626) 395-2129
Fax (626) 304-9834
E-mail: info@ligo.caltech.edu

Massachusetts Institute of Technology
LIGO Project, Room NW22-295
Cambridge, MA 02139
Phone (617) 253-4824
Fax (617) 253-7014
E-mail: info@ligo.mit.edu

LIGO Hanford Observatory
Route 10, Mile Marker 2
Richland, WA 99352
Phone (509) 372-8106
Fax (509) 372-8137
E-mail: info@ligo.caltech.edu

LIGO Livingston Observatory
19100 LIGO Lane
Livingston, LA 70754
Phone (225) 686-3100
Fax (225) 686-7189
E-mail: info@ligo.caltech.edu

http://www.ligo.caltech.edu/

1 Introduction

In the current LIGO design, 1064 nm light propagates through a Michelson interferometer and reflects off test masses [3]. Measurements of gravitational waves are made by analyzing the interference pattern that is output by the interferometer. The output is dependent on the phase difference between the beams in the two arms in the interferometer, and the lengths of the interferometer arms determine this phase shift. In order to accurately measure minuscule changes in the lengths of the interferometer arms, it is crucial to reduce various types of noise in the system, such as frequency noise. If a substantial amount of frequency noise is present in the laser that propagates through the system, it is difficult to differentiate changes in the interferometer output caused by gravitational waves from those caused by variations in the laser frequency.

Another source of noise in LIGO's data originates from the thermal noise of the test masses. LIGO's current test masses are made of fused silica, but mirrors made of crystalline silicon have demonstrated lower levels of mechanical loss than fused silica mirrors [6]. A decrease in mechanical loss will result in a decrease in thermal noise according to the fluctuation-dissipation theorem. Crystalline silicon is highly absorbent of 1064 nm light, but demonstrates low absorption of light in the range of 1400 - 2100 nm. Based on current laser technology, the best options for lasers in this range are 1550 nm or 1800 - 2100 nm lasers [1]. It is ideal to use a wavelength at the longer end of this range as crystalline silicon has lower absorption at longer wavelengths. Therefore, the next major upgrade of LIGO, LIGO Voyager, will likely switch to crystalline silicon mirrors and will use a wavelength of 2050 nm in the interferometer.

Access to low-cost sources of stable 2 μm light is crucial for researchers to develop the next generation of LIGO detectors. Many current methods of laser stabilization rely on reference cavities, which can be expensive and limit the laser frequency to the resonant frequencies of the cavity. A stabilization method that allows for many different wavelengths is advantageous, as semiconductor diode lasers have wavelength flexibility. This work will address the stabilization of a 2050 nm laser, and will focus on reducing the frequency noise of the laser with a self-delayed heterodyne interferometry technique. Our low-cost and flexible method has the potential to facilitate further testing and development of 2 μm light for gravitational-wave detection.

2 Approach

My setup is similar to the setup used in previous work on stabilizing a 1550 nm laser through self-delayed interferometry [2]. I will use a 2050 nm laser from Eblana Photonics, and an overview of my setup is displayed in Figure 1. First, the laser output will be split with a 90:10 fiber coupler. The 90% output will then be fed into a delay fiber while the 10% output will be fed into a fiber Mach-Zehnder interferometer. In this interferometer, the input is again split with a 50:50 coupler, with one output being fed into a 50:50 coupler while the other is fed through a piezo-driven General Photonics FPS-001 fiber stretcher (FS) and then into the 50:50 coupler. One output from the 50:50 coupler is transmitted to a photodetector (PD) which is a Thorlabs DET10D photodetector. Attached to the PD is a

trans-impedance amplifier with a 5 kΩ resistor. I will use our analog-to-digital converter (ADC), a Moku:Pro from Liquid Instruments, to translate the photodetector signal into a signal that will be fed into an Exail MPX2000-LN-0 electro-optic modulator (EOM) to produce a phase-corrected output, along with a signal that will be used to continually shift the FS such that the output of the interferometer is at a midpoint between constructive and destructive interference. The phase drift of the output from the EOM will be measured with another Mach-Zehnder interferometer setup, which will rely upon a simple delay fiber instead of an FS. This interferometer will be locked by modulating the resistance on the Thorlabs TED200C thermoelectric cooler (TEC) as changes in the TEC resistance manifest as changes in the laser wavelength. Once the EOM-corrected frequency noise from the second interferometer is measured I will compare the two measurements of the frequency noise to analyze the efficacy of the EOM correction.

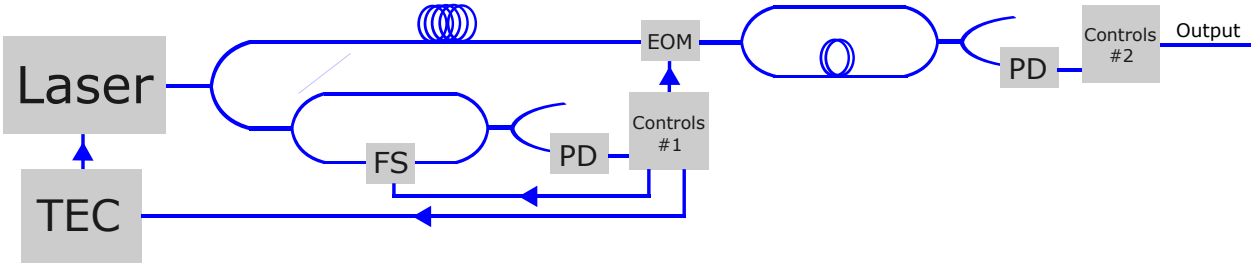

Figure 1: A diagram of my setup.

Before beginning to work in the laboratory, I worked on calculating how different sources of laser noise would appear on our PD output signal. Say we have an initial input into the interferometer of

$$E_{in}(t) = Ae^{i(\omega_0 t+\phi_n(t))}$$

This is split by the first 90:10 splitter then a 50:50 splitter, which each have losses of 2 dB, to get two inputs to the FS interferometer of

$$e_A(t) = 10^{\frac{-4}{20}} A\sqrt{\frac{1}{20}}e^{i(\omega_0 t+\phi_n(t))}, e_B(t) = i10^{\frac{-4}{20}} A\sqrt{\frac{1}{20}}e^{i(\omega_0 t+\phi_n(t))}$$

Say that it takes τ to propagate through the arm of the interferometer which has the FS, the fibers have an attenuation coefficient of α, and the FS has a loss of 6 dB. Then, the two signals going into the second 50:50 splitter will be

$$E_1(t) = 10^{\frac{-4}{20}} e^{-\alpha L} A\sqrt{\frac{1}{20}}e^{i(\omega_0 t+\phi_n(t))}, E_2(t) = i10^{\frac{-10}{20}} e^{-\alpha L} A\sqrt{\frac{1}{20}}e^{i(\omega_0 t-\omega_0\tau+\phi_n(t-\tau))}$$

where L is the length of the fiber through which the signal travels (not including the length of the FS).

If the second 50:50 coupler has a loss of 2 dB and we define constants of

$$C_A = 10^{\frac{-6}{20}} e^{-\alpha L} A\sqrt{\frac{1}{40}}, C_B = 10^{\frac{-12}{20}} e^{-\alpha L} A\sqrt{\frac{1}{40}}$$

then the two outputs are

$$E_3(t) = C_A e^{i(\omega_0 t + \phi_n(t))} - C_B e^{i(\omega_0 t - \omega_0 \tau + \phi_n(t-\tau))}$$

$$E_4(t) = iC_A e^{i(\omega_0 t + \phi_n(t))} + iC_B e^{i(\omega_0 t - \omega_0 \tau + \phi_n(t-\tau))}$$

with intensities of

$$I_3(t) = C_A^2 + C_B^2 - 2C_A C_B cos(-\omega_0 \tau + \phi_n(t-\tau) - \phi_n(t))$$

$$I_4(t) = C_A^2 + C_B^2 + 2C_A C_B cos(-\omega_0 \tau + \phi_n(t-\tau) - \phi_n(t))$$

$\phi_n(t) - \phi_n(t-\tau)$ will be shortened to $\Delta\phi(t)$, and assuming $\Delta\phi(t)$ is small, then

$$cos(\omega_0 \tau + \Delta\phi(t)) \approx cos(\omega_0 \tau) - \Delta\phi(t) sin(\omega_0 \tau)$$

As detailed in Section 3, we will create a control system that sets $\omega_0 \tau = 2\pi n + \frac{\pi}{2}$ such that

$$cos(\omega_0 \tau) = 0, sin(\omega_0 \tau) = 1$$

Then, the output intensities are

$$I_3(t) = C_A^2 + C_B^2 + 2C_A C_B \Delta\phi(t)$$

$$I_4(t) = C_A^2 + C_B^2 - 2C_A C_B \Delta\phi(t)$$

If we consider amplitude fluctuations ($A(t) = A_0 + dA(t)$) and we define constants

$$C_0 = \frac{A_0^2 10^{\frac{-6}{10}} e^{-2\alpha L}}{40}(1 + 10^{\frac{-6}{10}})$$

$$C_1 = \frac{2A_0 10^{\frac{-6}{10}} e^{-2\alpha L}}{40}(1 + 10^{\frac{-6}{10}})$$

$$C_2 = \frac{10^{\frac{-18}{20}} e^{-2\alpha L} A_0^2}{20}$$

The output intensities are

$$I_3(t) = C_0 + C_1 dA(t) + C_2 \Delta\phi(t) \quad (1)$$

$$I_4(t) = C_0 + C_1 dA(t) - C_2 \Delta\phi(t)$$

3 Locking the Fiber Stretcher Interferometer

As the length delay τ between the arms in our FS interferometer varies linearly, the intensity of the output signal will vary sinusoidally. The principle of locking an interferometer revolves around using a control system that continually sets the output of the interferometer to a particular point of the sinusoidal output.

For example, as we apply a triangular wave to the FS with the Moku output, we can push the output of the FS interferometer through fringes, as shown in Figure 2.

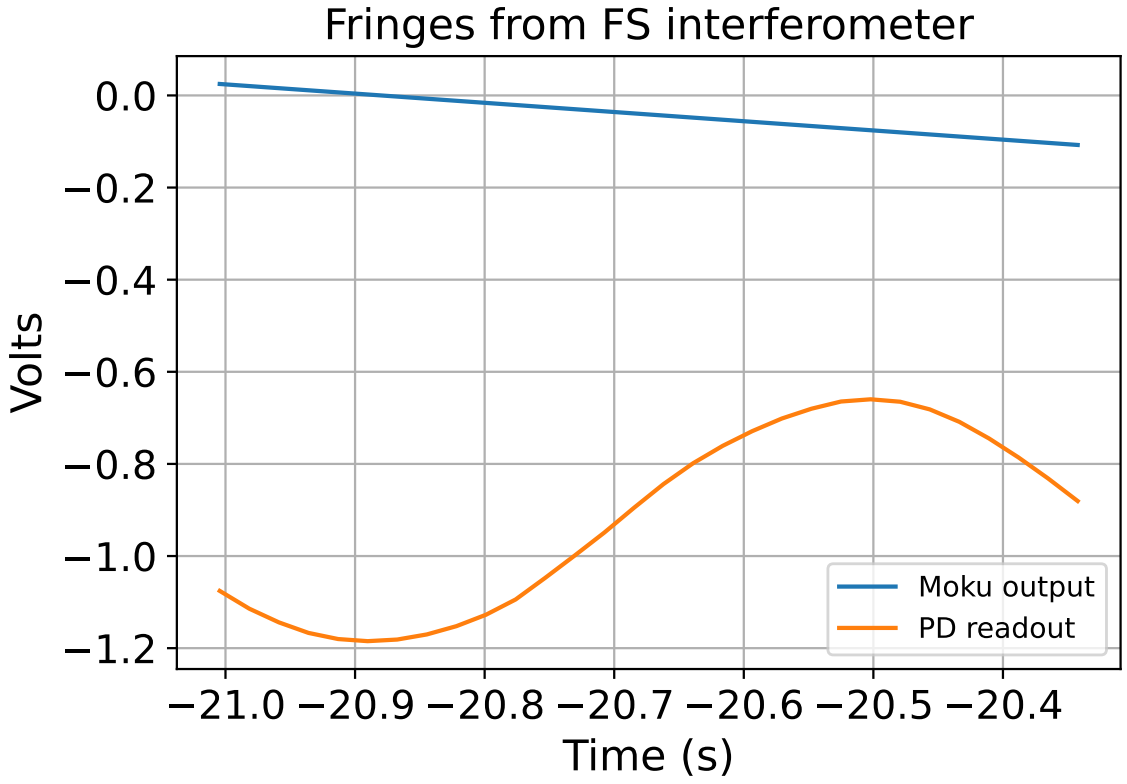

Figure 2: Output of the FS interferometer as it is pushed through fringes.

We chose to lock the output to the midpoint of the fringe which would be around -0.9 V in Figure 2. This point lies in the linear regime of the output, meaning that small phase changes will be linearly related to the interferometer output. Therefore, once the interferometer is locked to the midpoint, we will be able to measure the phase noise of our laser.

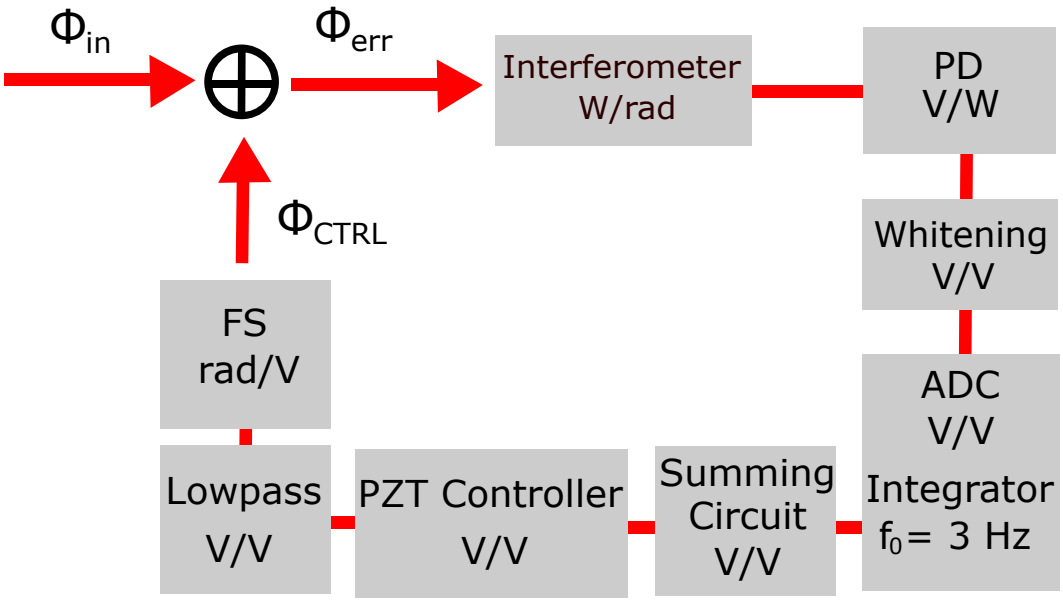

Figure 3: A diagram of the control loop we are using the lock the FS interferometer.

As displayed in Figure 3, we use the signal output by the FS interferometer to create a signal that drives the FS, pushing the output of the interferometer back to the midpoint. More specifically, we read the output of the interferometer with a PD. After the PD, we use a whitening filter that amplifies all signals going into the ADC in a certain frequency band in order to limit the impact of the noise floor of the ADC. On the ADC, we set the PID instrument to have an integrator filter with a gain of 1 dB at around 3 Hz, which allows us to correct the low-frequency drift of the output while suppressing extraneous signals at high frequencies. We then use a piezo (PZT) controller to amplify the signal from the ADC by a factor of 15 in order to access the full range of our FS. However, the signal produced by the ADC is in the range of ±5 V, and the PZT controller takes inputs of 0-150 V. Therefore, we constructed a summing circuit to translate the ADC output signal to a signal in the range of 0 - 10 V.

3.1 Whitening Filter

Our whitening filter was adapted from a previous design [5]. We constructed this whitening filter with the goal of amplifying the signal in the mid-frequency range, and suppressing the signal at high and low ranges of our frequency band.

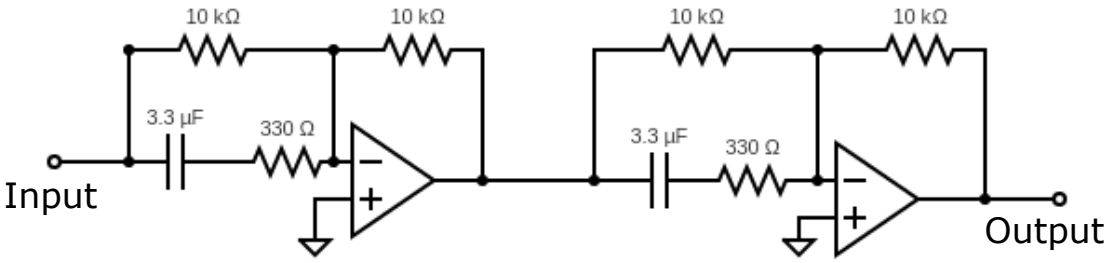

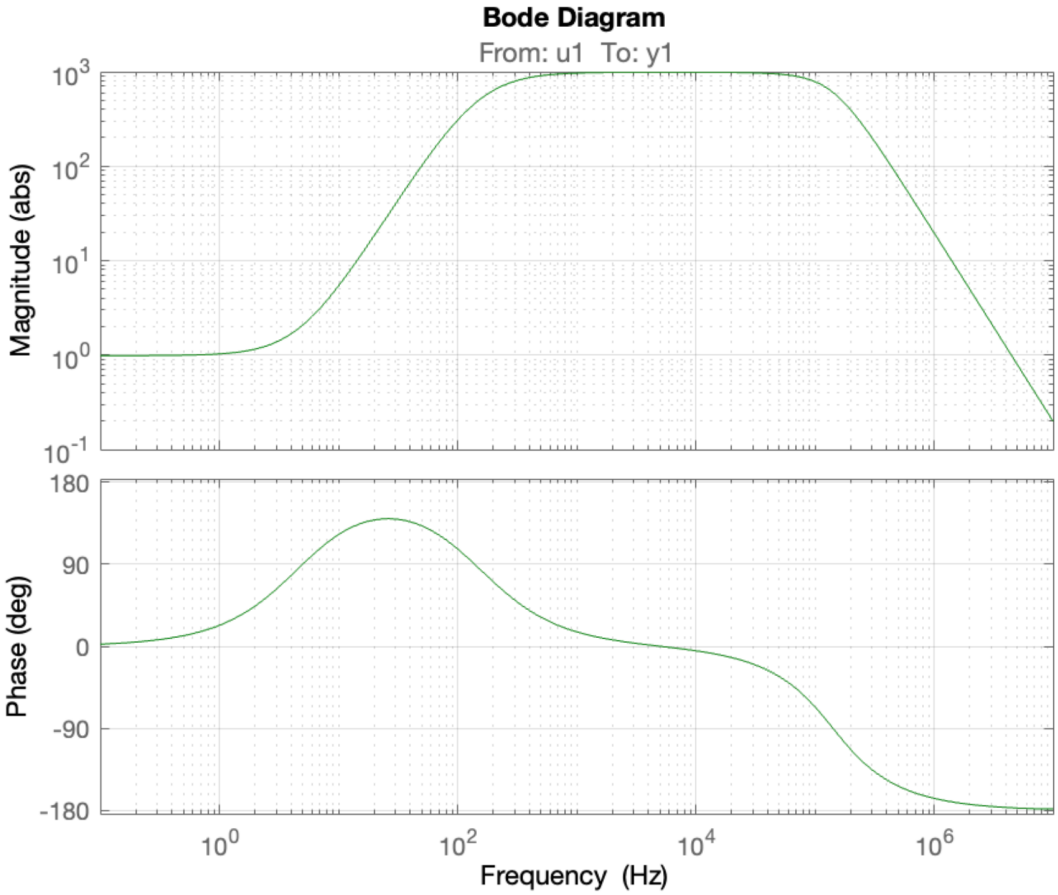

Figure 4: A circuit diagram and Bode plot of our whitening filter.

3.2 Summing Circuit

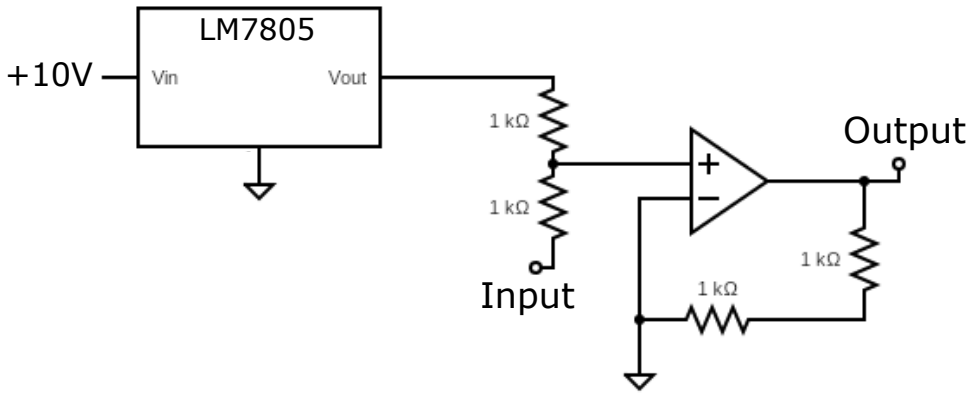

Figure 5: A circuit diagram of our summing circuit.

This circuit adds 5 V to the voltage that is input.

3.3 Lowpass Filter

The lowpass filter we constructed consists of two 75 kΩ resistors in series. The output of the PZT controller has a resistance of 150 Ω and the FS has a capacitance of 190 nF. Therefore, the filter theoretically has a cutoff at 5.6 Hz. In order to test the response of the filter, I used the PID instrument and the frequency response analyzer instruments at the same time on the ADC in order to lock the loop while finding a transfer function between the signal output by the interferometer and the signal output by the ADC. I added both signals together with an SR560, and the sum was fed into the FS.

In Figure 5, there is a section with flat gain in the "no filter" measurement from about 50 Hz - 50 kHz. We subtracted this flat gain value from the filter measurement in order to find a transfer function of only the lowpass filter. Then, we fit the "filter" measurement with a function of the form

$$G(f) = 10 \log_{10} \left(\frac{1}{1 + \frac{f^2}{\omega_0^2}} \right)$$

from 10 Hz - 1 kHz to find a cutoff at $\omega_0 = 6.6$ Hz. At higher frequencies, our measurement was hitting the ADC noise floor so we excluded the data from the fit.

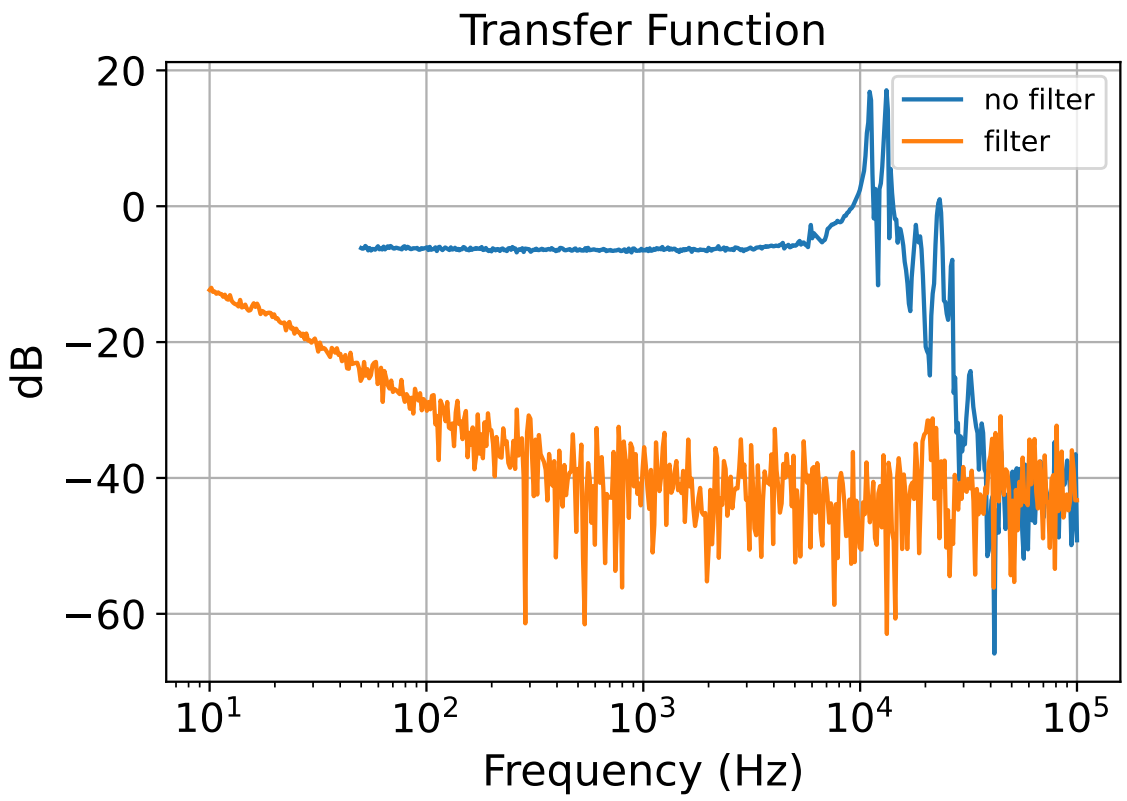

Figure 6: The measured transfer functions of the output to the interferometer to the ADC's output swept sine wave, measured with and without the lowpass filter.

4 Calibrating the Photodiode

We needed to find a calibration factor that related the intensity of the signal input to the PD to the voltage output by the PD. To do this, we noted that if we measured the laser signal with the PD and the laser power was large enough, the intensity noise of the laser would dominate the PD output at low frequencies and the shot noise would dominate at high frequencies. Shot noise arises in our photodetector due to the fact that the photocurrent is comprised of the flow of discrete electrons, and thus there are variations in the number of electrons flowing per unit time as governed by Poisson statistics. We can calculate the amplitude spectral density of the shot noise that is present in our photodiode across all frequencies with

$$n_{shot}(f) = \sqrt{2qI} \tag{2}$$

where I is average photocurrent in the photodiode and q is the charge of the electron.

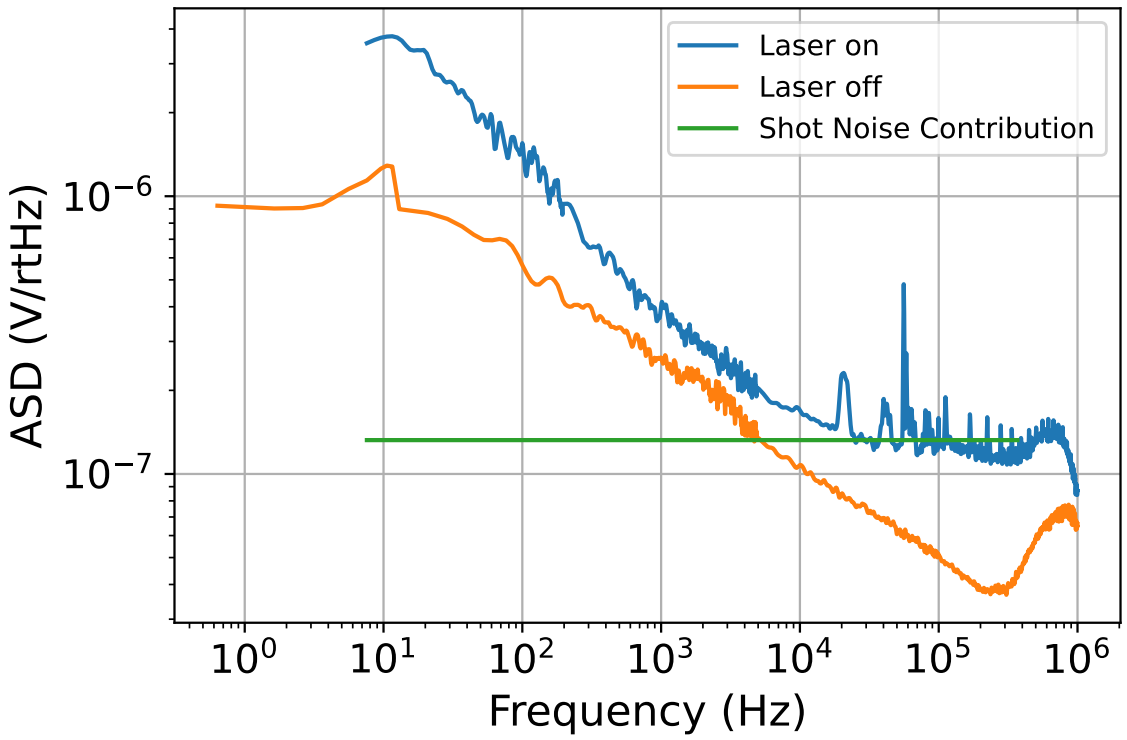

Figure 7: Data from the PD with the laser on and off.

Since we expect the shot noise to have a flat spectrum as it is not frequency dependent, we can see the shot noise dominating in the range of about 10 kHz - 500 kHz of the "Laser on" measurement in Fig 7. Then, we estimated the contribution of shot noise to the output in terms of $\frac{V}{\sqrt{Hz}}$. We can also calculate the shot noise spectrum in the PD in terms of $\frac{Amps}{\sqrt{Hz}}$ with Eq. 2, and convert this value to $\frac{W}{\sqrt{Hz}}$ based on the responsivity of the PD. Then, we divide the output flat value by the shot noise spectrum to find a calibration factor in terms of $\frac{V}{W}$.

5 Noise Budget

LIGO utilizes a method called "noise budgeting" to compare the signal of the measured strain in the interferometer arms to how different sources of noise in the instrument appear as a strain. I used a similar method in order to compare my measurement of frequency noise to how different sources of noise would appear as frequency noise. With this method, we can perform a signal-to-noise comparison and find the frequency bands in which we are able to make reliable measurements.

5.1 Calibration

In order to calibrate each noise source to frequency noise, we applied a triangular wave to the FS in order to push the output of the FS interferometer through multiple fringes, as displayed in Figure 2. Since all of our noise measurements are in terms of voltage (V), we are interested in finding a $\frac{rad}{V}$ calibration. We take the slope of the fringe at its midpoint in order to find a calibration in terms of $\frac{V}{sec}$. Then, we can look at the amount of time it takes to sweep through π radians, which is the time from crest to peak to find a factor in terms of $\frac{rad}{sec}$. Then, we can divide these two factors to find our calibration factor in terms of $\frac{rad}{V}$. We then convert from phase noise to frequency noise within the interferometer from the conversion

$$\Delta\phi = 2\pi\tau\Delta f$$

where τ is the time delay in the interferometer.

In Figure 2, the slope of the PD readout at the midpoint is 2.24 $\frac{V}{sec}$, and it takes to 0.36 seconds sweep through π radians. Therefore, we find a conversion factor of 3.67 $\frac{rad}{V}$. We estimate the time delay in the interferometer based on the fact that the length of the fiber in the FS is about 2 m, and that the fibers have a refractive index of about n=1.5. Therefore,

$$\tau \approx \frac{2n}{c}$$

and with our two conversion factors we can calibrate voltage measurements to apparent frequency noise. Once we find the apparent frequency noise of all our sources of noise, we add them in quadrature to find the total noise.

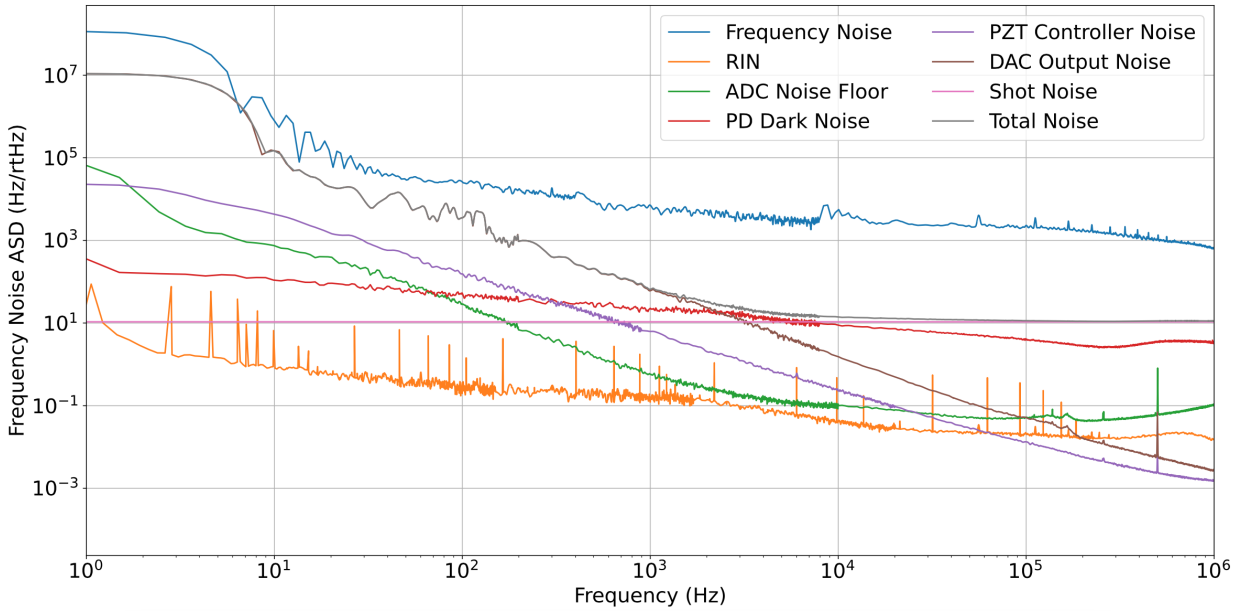

Figure 8: My noise budget with all the sources of noise that we are considering.

5.2 Frequency Noise

Once our interferometer output was locked to the middle of a fringe, we measured the spectrum of the output of the PD with the ADC, and converted the voltage measurement into frequency noise.

5.3 Relative Intensity Noise

The other notable source of noise arising from the laser output is the relative intensity noise (RIN). We measured the RIN of our laser by simply measuring the direct output of the laser with a PD, bypassing the interferometer. This gave us a measurement of the spectrum of the intensity noise in terms of $\frac{V}{\sqrt{Hz}}$, which we could convert to $\frac{W}{\sqrt{Hz}}$ by dividing by the photodiode calibration factor. Then, we divide by the intensity of the laser in order to obtain the relative intensity noise in terms of $\frac{1}{\sqrt{Hz}}$. To then convert measured intensity noise to apparent intensity out of the interferometer, we used the term $C_1 dA(t)$ from Eq. 1, and then converted this to voltage out of the PD using the PD calibration factor, which we then converted back to frequency noise.

5.4 ADC Noise Floor and Whitening Filter

The noise in our ADC arises from the fact that there is noise inherent in the internal electronics. We found the equivalent frequency noise of our ADC noise floor by terminating all of its inputs and outputs and then converting the measured output voltage back into frequency noise. The ADC noise floor displayed in Figure 8 is not a raw measurement, but has the inverse gain of our whitening filter applied, as the filter amplifies all signals other than the ADC floor.

5.5 PD Noise

There is also noise present in our system due to the fact that when we apply a bias voltage to the photodiode, there is a small amount of current leakage in the detector which manifests as small voltage fluctuations measured on the Moku. This noise is called PD dark noise and is present regardless of whether the laser is on or off. We measured the dark noise of our PD by turning the detector on with the laser off, and monitoring the output on the Moku.

5.6 Shot Noise

There is also shot noise in our photodiode, which has already been described in Section 4.

5.7 PZT Controller and ADC Output Noise

We have noise in our system arising from the process of creating a signal that drives our PZT. One source of this noise is from creating a control signal with our Moku. We measured this small signal noise by configuring the Moku to output a low amplitude and frequency sine wave and then measuring the spectrum of the output. In addition, there is noise in the

output of the PZT controller. We measured this noise by inputting a DC signal into the controller and measuring the spectrum of the output.

6 Locking the TEC Interferometer

We also locked the output of the second interferometer, which is the interferometer we are using to measure the success of our correction with the EOM. Initially, we planned to lock this interferometer by directly controlling the temperature of the delay fiber. We tried wrapping part of the fiber around a Peltier tile which would heat up or cool down, thereby adjusting the length of the fiber and adjusting the phase shift. However, we were unable to change the temperature of the fiber quickly enough. Instead, we modulated the resistance setting of our TEC controller, which would thereby modulate the wavelength output by the laser. Our control system is depicted in Figure 9.

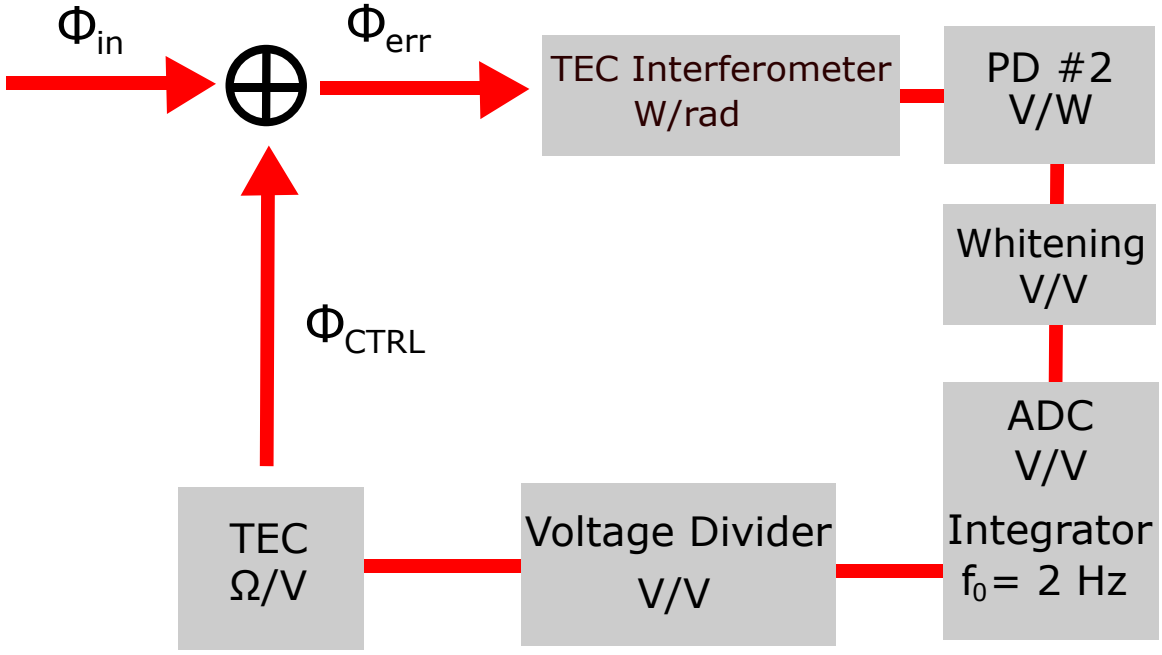

Figure 9: Our control system for locking the second interferometer.

Our voltage divider was created because the output voltage from the ADC was too large of a voltage to apply to the TEC in order to create the necessary voltage changes. The circuit divided the output Moku voltage by 100 at low frequencies. The gain was smaller at higher frequencies because the TEC did not respond to high-frequency resistance variations.

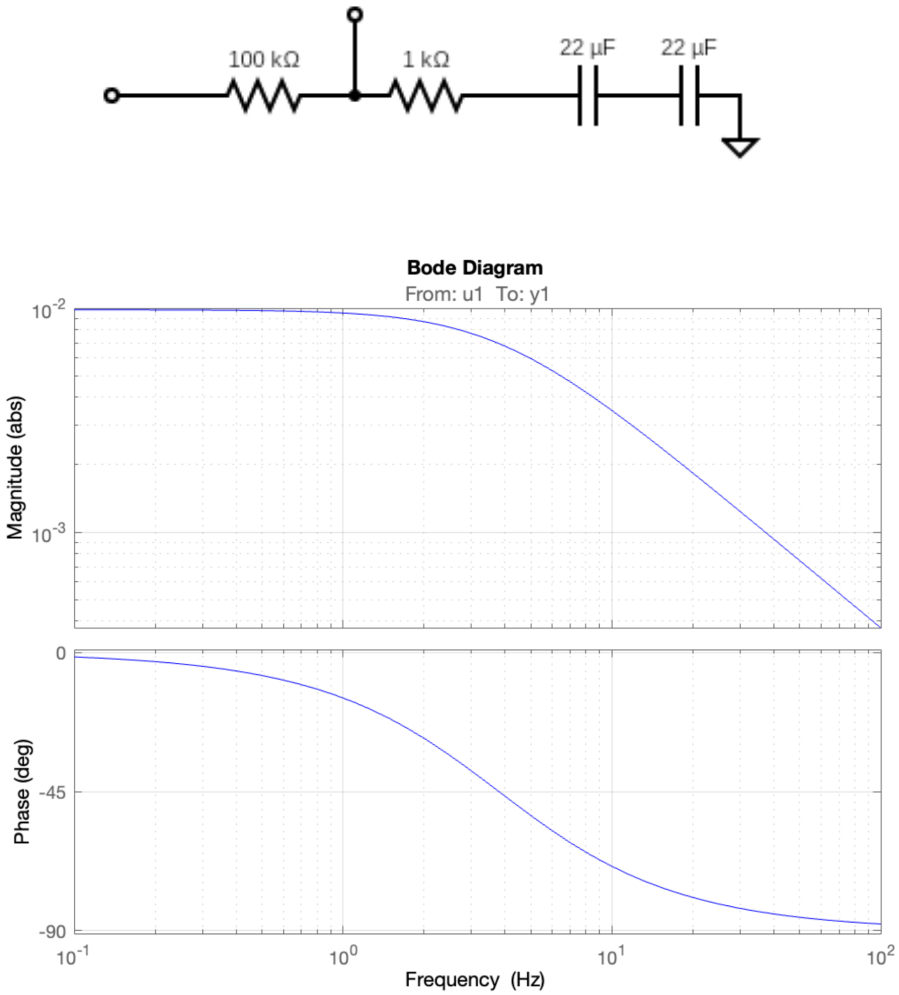

Figure 10: A circuit diagram and Bode plot of our voltage divider circuit.

7 Performing the Feedforward

7.1 Measuring the ADC Delay

In order to obtain the best result with our feedforward, we hoped to match the time delay in our fiber that leads directly to the EOM with the time it takes for a signal to travel through our FS interferometer and be converted to an ADC output. The main source of delay in our system originated from creating a signal with the ADC. We performed a swept sine analysis with a Zurich Instruments HF2 Lock-In Amplifier to measure the delay in the PID filter, FIR filter builder, and the digital filter box instruments on both a Moku:Pro and a Moku:Go. We noticed linear trends in the phase change on our Bode plots, and we could relate the phase ϕ, frequency f, and time delay τ_{ADC} with

$$\phi(t) = \tau_{ADC} f + \phi_0$$

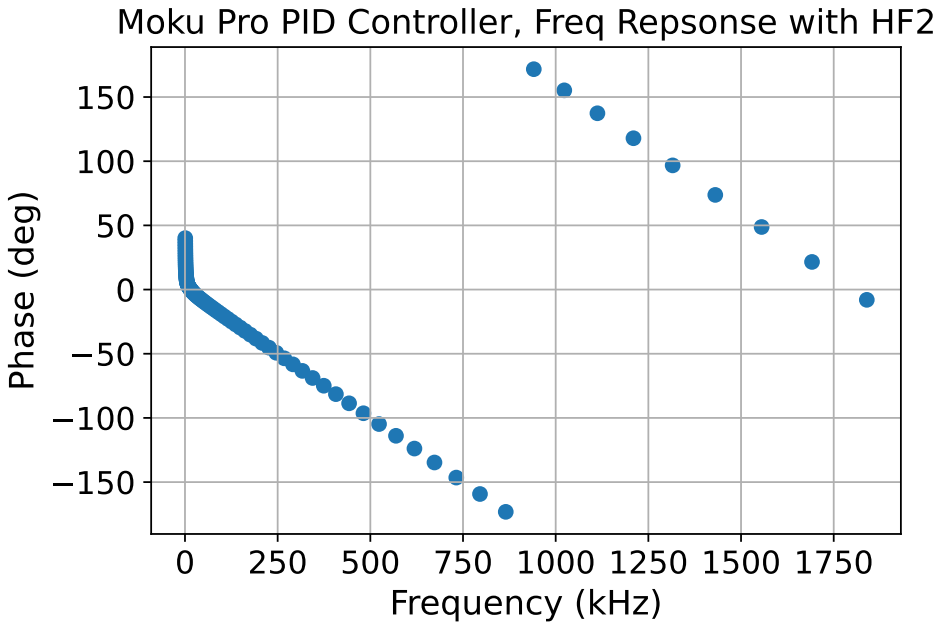

Figure 11: The measured phase delay from the PID instrument on the Moku:Pro.

The Moku:Pro PID instrument has the smallest delay of 546 ns. In order to match this delay with a delay fiber, we would need a length of about 160 meters, calculated with

$$L = \frac{\tau_{ADC} c}{n}$$

where $n \approx 1.5$ in our fibers. We did not have a fiber this long, so we used our longest fiber of 15 m instead.

7.2 Controlling the EOM

We used the digital filter box instrument on the ADC to apply a fourth-order Gaussian filter to the output of the FS interferometer. The DAC output was then fed through a buffer amplifier which was an SR560 with a flat gain of 1, and then into the EOM.

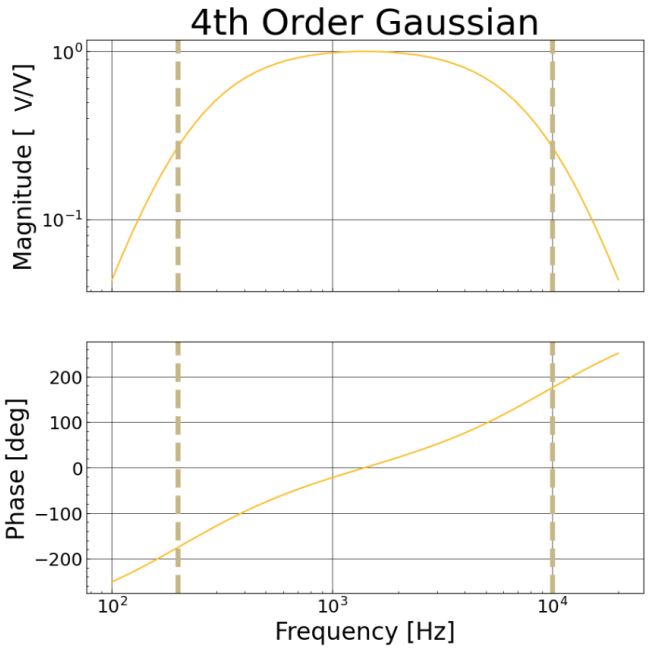

Figure 12: The transfer function of our ADC filter, which created the signal going into the EOM.

We also measured the transfer function of our EOM by locking both interferometers and performing a frequency response analysis between the input to the EOM and the output of the TEC interferometer PD.

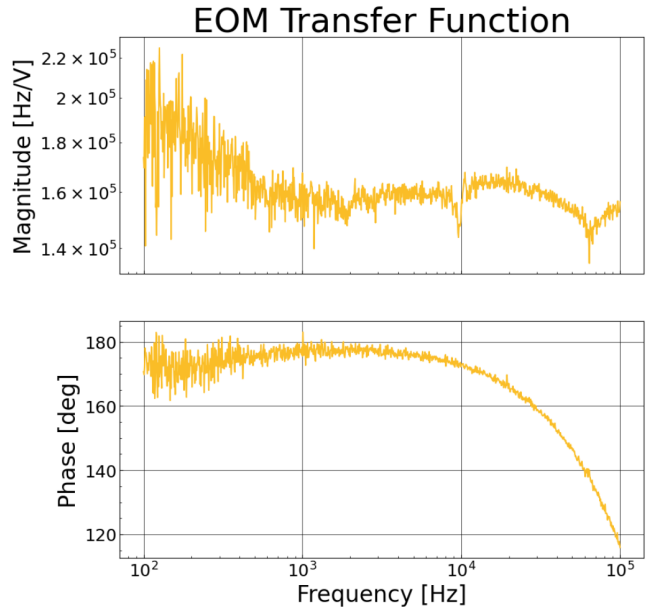

Figure 13: The transfer function between the input voltage to the EOM and the output modulation signal.

8 Results

After we performed the feedforward with the EOM, we obtained an output signal from the TEC interferometer, and we calibrated the output of this signal to frequency noise using the method described in Section 5.1. Figure 14 illustrates the frequency noise measured at the output of the TEC interferometer with the EOM applying a correction signal ("Correction On") and with the EOM applying no signal ("Correction Off"). We can see that the frequency noise has been corrected in a band from around 2 - 5 kHz.

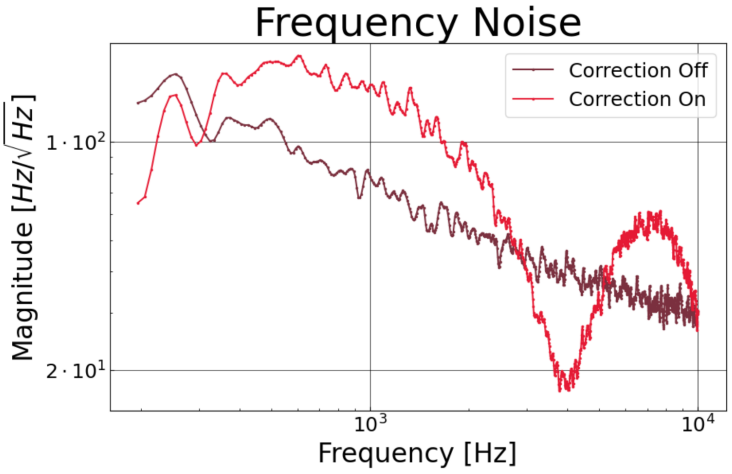

Figure 14: Our frequency noise measurements at the TEC interferometer output.

9 Future Work

One of the main concerns we have with our current setup is that we have not matched the Moku electronics delay with the delay in the signal that is fed into the EOM to be corrected. If we wanted to buy the 160 m of fiber that is necessary to match our electronics delay, it would cost about $3500 from Thorlabs. With our current 15 m fiber, we can allow for an electronics delay of 80 ns. An alternative to the Moku:Pro that we considered was using a Red Pitaya. However, the delay of the Red Pitaya is around 400 ns, which would not be a large improvement over the Moku:Pro [7]. The next alternative would be to perform the filtering in analog. Previous work on feedforward laser stabilization has demonstrated that analog circuitry used to detect phase error and then apply a signal to an EOM has a delay of 140 ns, which is much closer to our ideal delay [4].

In addition, we believe that our correction results would be improved with more time spent tuning the ADC filter that creates a signal to the EOM. We were unable to spend much time on this aspect during the SURF program due to time constraints. However, if we spent more time tuning the high and low-frequency cutoffs of our bandpass filter, we would likely be able to improve our output.

We also have more work to do with regard to considering other sources of noise in our measurement. For example, we have not yet calculated how noise in the signal we are

using to modulate the TEC resistance would manifest as noise in the output of the laser. In addition, it would be prudent to consider thermal and acoustic noise in our analysis. Another thing to consider is that the EOM has the possibility of inducing amplitude modulations on its output signal.

10 Acknowledgements

I would like to thank my mentors, Dr. Aidan Brooks and Dr. Rana Adhikari for their guidance and support. I would also like to thank my colleague Hannah Rose for her invaluable contributions to this project. In addition, I would like to thank Alan Weinstein for organizing the SURF program. This work was supported by the National Science Foundation Research Experience for Undergraduates (NSF REU) program, the LIGO Laboratory Summer Undergraduate Research Fellowship program (NSF LIGO), and the California Institute of Technology Student-Faculty Programs.

References

[1] R X Adhikari et al. A cryogenic silicon interferometer for gravitational-wave detection. *Classical and Quantum Gravity*, 37(16):165003, Jul 2020.

[2] Jiageng Chen, Qingwen Liu, and Zuyuan He. Feedforward laser linewidth narrowing scheme using acousto-optic frequency shifter and direct digital synthesizer. *Journal of Lightwave Technology*, 37(18):4657–4664, 2019.

[3] LIGO Scientific Collaboration. Advanced LIGO. *Classical and Quantum Gravity*, 32(7):074001, Mar 2015.

[4] Lintao Li, William Huie, Neville Chen, Brian DeMarco, and Jacob P. Covey. Active cancellation of servo-induced noise on stabilized lasers via feedforward. *Physical Review Applied*, 18(6), dec 2022.

[5] Simona Miller, James Lough, and Nikhil Mukhund. *Improved Whitening of the Readout Signal for GEO 600*, Jul 2019.

[6] J. Steinlechner, I. W. Martin, A. S. Bell, J. Hough, M. Fletcher, P. G. Murray, R. Robie, S. Rowan, and R. Schnabel. Silicon-based optical mirror coatings for ultrahigh precision metrology and sensing. *Phys. Rev. Lett.*, 120:263602, Jun 2018.

[7] Alex Tourigny-Plante, Vincent Michaud-Belleau, Nicolas Bourbeau Hé bert, Hugo Bergeron, Jérôme Genest, and Jean-Daniel Deschênes. An open and flexible digital phase-locked loop for optical metrology. *Review of Scientific Instruments*, 89(9), sep 2018.